Journal of Nuclear Materials 390–391 (2009) 88–91

Contents lists available at ScienceDirect

Journal of Nuclear Materials

journal homepage: www.elsevier.com/locate/jnucmat

Transfer of rovibrational energies in hydrogen plasma–carbon surface interactions

P.S. Krstic [a,*], E.M. Hollmann [b], C.O. Reinhold [a], S.J. Stuart [c], R.P. Doerner [b], D. Nishijima [b], A.Yu. Pigarov [b]

[a] Oak Ridge National Laboratory, Physics Division, P.O. Box 2008, Oak Ridge, TN 37831-6372, USA
[b] University of California, San Diego, CA, USA
[c] Clemson University, Department of Chemistry, Clemson, SC 29634, USA

ARTICLE INFO

PACS:
52.40.Hf
34.50.Ez
34.35.+a

ABSTRACT

We present state-of-the-art molecular dynamics (MD) simulations of high-density plasma-bombardment of carbon, mimicking plasma–wall interactions at the fusion reactor first wall. Bare and hydrogenated amorphous carbon surfaces with temperatures in the range of 300–800 K are bombarded by a distribution of neutral hydrogen molecules representing well-defined center-of-mass and rovibrational temperatures. The MD simulations are benchmarked against experiments in which a heated carbon surface is irradiated with hydrogen molecules from a plasma source. Comparisons between simulations and experiment are presented for the rovibrational distributions upon reflection and the rotational and vibrational accommodation coefficients.

1. Introduction

Since plasma-boundary physics encompasses some of the most important unresolved issues in future energy production for fusion reactors, there is a strong interest in the fusion community for better understanding and characterization of plasma–surface interactions. These interactions lead to surface erosion and particle deposition, which degrades fusion performance and produce long-term particle retention.

Motivated by this need, we have recently undertaken a series of large-scale classical molecular dynamics (MD) simulations of particle–surface interactions involving carbon surfaces. Our previous calculations were focused on modeling chemical sputtering, implantation, reflections and dissociation processes of hydrogenated carbon from well-defined low-intensity ion beam experiments [1–3]. In this work we extend our previous approach to model a high-density plasma-bombardment environment. Our simulation results are directly compared with carefully designed plasma irradiation experiments performed at the University of California (San Diego) [4–8]. In Section 2 we describe our MD simulations of the plasma-facing surfaces. In Section 3 we describe the experimental setup in some detail. Both experimental and theoretical results and our discussion are presented in Section 4.

2. Theory

Details of our classical MD approach, as well as of the bond order REBO potential, can be found in previous publications (see [1–3] and references therein). Here we describe only the new aspects needed to model plasma experiments, i.e. the randomization of the simulated impact parameters to represent a plasma. Our previous studies have shown [1–3] that the best agreement with experiments [3] is reached when the surfaces are prepared by bombardment, closely mimicking the experiments, until a 'steady-state surface' is reached. Applying this prescription to a surface irradiated by plasma requires that the impact particles have the proper distributions of energy, angle, position, angular momentum, during both the preparation of the surfaces and the calculation of the particle emission yields.

2.1. Sampling initial conditions for H_2 molecules in the plasma

Clearly, to sample initial conditions one can separate the internal degrees of freedom (relative position and momentum $\vec{r},\vec{p}$) and the translational center-of-mass (c.m.) degrees of freedom $(\vec{r}_{cm},\vec{p}_{cm})$ of the diatomic molecule. Initial conditions can be sampled from a probability density

$$\rho_{cm}(\vec{r}_{cm},\vec{p}_{cm})\,\rho_{\mathrm{int}}(\vec{r},\vec{p})$$

The phase space coordinates have to be sampled through distributions that depend only on the constants of motion of the system in order to obtain a stationary distribution. In our case these are

* Corresponding author.
E-mail address: krsticp@ornl.gov (P.S. Krstic).

0022-3115/$ - see front matter © 2009 Elsevier B.V. All rights reserved.
doi:10.1016/j.jnucmat.2009.01.096

$\vec{p}_{cm}$, $H_{\rm int}$, $\vec{L}$, where $H_{\rm int}$ is the Hamiltonian of rovibrational motion and L is the angular momentum. For the c.m. coordinates, sampling is relatively simple and one can use $\rho_{cm}(\vec{r}_{cm},\vec{p}_{cm}) = \delta(z_{cm}-z_0)U(x_{cm})U(y_{cm})\rho^{Max}_{T_t v_0}(\vec{p}_{cm})$, where z_0 is the initial z position of the c.m. along the surface normal, x_{cm} and y_{cm} are sampled uniformly, and $\vec{p}_{cm}$ is sampled from a shifted Maxwell–Boltzmann distribution $\rho^{Max}_{T_t v_0}(\vec{p}_{cm})$ with mean velocity v_0 and translational temperature T_t, and $U(x)$ is a uniform distribution in x. For the internal degrees of freedom, a stationary distribution is $\rho_{\rm int}(\vec{r},\vec{p}) = \rho_{\rm int}(H_{\rm int},\vec{L}) = \rho_{vib}(H_{\rm int})\rho_{rot}(L)U(\hat{L})$, where $U(\hat{L})$ is a uniform distribution for the direction of the angular momentum of the molecule (in the unit sphere), and $\rho_{vib}(H_{\rm int}), \rho_{rot}(L)$ are Boltzmann distributions for the 'vibrational' and 'rotational' degrees of freedom. We first sample L from $\rho_{rot}(L)$, use the chosen L value into $\rho_{vib}(H_{\rm int})$ to get (r,p_r) and then calculate $p_\perp = L/r$. In order to mimic the experiment, we use a Maxwell distributions with center-of-mass temperature of T_t = 800 K, while the internal temperatures distributions were chosen with 3000 K for rovibrational motion (i.e. 5000 K for vibrational temperatures) and 1000 K for rotational motion. This lack of equilibrium between rotational and vibrational temperatures is the best estimate of the experimental conditions in the considered non-equilibrium plasma with short confinement times.

2.2. Preparation of the target surface

The target surfaces in our MD simulations are bare and hydrogenated amorphous carbon (a-C:H). This reflects the fact that the graphite divertor target in the experiment was polycrystalline POCA graphite surface, without a well-defined direction of the basal plane. The experiment implies long plasma exposure times and therefore a possibility of hydrogenation of the surface. Although the bulk material is known to have a H:C ratio of 0.4 at saturation level, simulations have shown that at low impact energies this ratio can be substantially elevated at the interface [1–3]. Since the level of hydrogenation in the experiment is not known, we use both bare (non-hydrogenated) surfaces as well as a-C:H surfaces exposed to varying levels of fluence with a 1 eV beam. Building hydrogenated surfaces for all possible plasma parameters would have involved a bigger effort. However, the approach we undertook gave us a clear answer on the role of the hydrogenation. In order to speed up the hydrogenation the surfaces were prepared by cumulative bombardment of an initial surface of 1750 carbon atoms and 700 hydrogen atoms, with carbon density of 2 g/cm^3 and at 300 K, homogeneously hydrogenated at a H:C ratio of 0.4. These were then equilibrated at various temperatures (300, 400, 600 and 800 K), using a Langevin thermostat. Five surfaces were prepared at fluences of 100, 200, 400, 800 and 1200 impacts of H_2 molecules on a surface cell with dimensions of 10 Å $\times$ (26.5 Å)^2, which reflect various levels of hydrogenations at the surface. The two higher fluences are enough that the surface has entered a steady-state regime, and surface composition changes little with subsequent impacts.

2.3. Simulation procedure

For each surface, defining a hydrogenation level, and for each surface temperature, the irradiation is repeated for 1000 random independent trajectories. The c.m., rotational, rovibrational and vibrational energies and corresponding kinetic temperatures were determined for each reflected H_2 molecule, and averaged over all trajectories. The number of trajectories for each surface was satisfactorily large, resulting in less than 5% statistical uncertainty (one standard deviation) of the calculated averages.

3. Experiment

The PISCES-A reflex-arc plasma discharge [4] is used to create rovibrationally excited hydrogen molecules which fill a vacuum chamber. These H_2 neutrals travel down a stainless steel side port and then enter a small graphite tube mounted in the side port. An electron beam is aimed down the hollow graphite tube to electronically excite a small fraction of the hydrogen molecules inside the tube. The resulting line emission is then measured at 4 positions in the tube. The local H_2 ground electronic state vibrational and rotational temperatures T_{vib} and T_{rot} at each fiber location can then be calculated with measured line ratios of H_2 Fulcher band emission [5,6]. Additionally, the H_2 kinetic temperature T_{kin} and density n_{H2} can be obtained from line broadening and line intensity, respectively.

A detail of the graphite tube arrangement is shown in Fig. 1 (for simplicity, the adjacent plasma discharge is not shown here). Collimator lenses are used to increase the amount of light gathered into the four fibers. Heater wire wrapped around the graphite tube is used for heating. The graphite tube temperature (assumed to be uniform) is measured with a thermocouple at the end of the tube. The graphite tube is made of E-294 graphite from Electro-Tech Machining with density $\rho = 1.80$ g/cm^3 and average grain size of 0.10 mm. The tube dimensions are: length L = 10 cm, diameter D = 3.8 cm, and thickness t = 0.64 cm. Prior to taking data, the graphite was baked out for 4 h at 1000 °C to remove stored water. The graphite was not exposed to plasma prior to the experiments, so hydrogen in the walls arrives as neutrals, not as embedded ions.

The electron beam is created using a D = 1.2 mm Ta disk cathode emitter. Typical beam energies are 70 eV; this is chosen to be well above the threshold for H_2 electronic excitation ($\sim$10 eV) so that signal brightness is not sensitive to small changes in beam energy. Beam currents ($\sim$1 mA) are small and heating of H_2 in the tube due to the beam is found to be negligible.

4. Results and discussion

Typical for all calculations performed here is that the results for hydrogenated surfaces are different from the results with the bare carbon surface. Fig. 2 shows the average temperatures of various modes of motion for H_2 after reflection from the surface. The initially similar values of rotational and c.m. temperatures (1000 K and 800 K) lead to very similar values of the final temperatures (the results for hydrogenated surfaces lie within the same depicted shaded area). However, the reflected H_2 is typically 'hotter' both rotationally and translationally for the hotter surfaces, and hotter for the bare than for the hydrogenated surfaces, becoming cooler with increased hydrogenation (arrow in Fig. 2). On the other hand, the vibrational temperature is significantly decreased in the collision, though no clear trend is found with the hydrogenation level. These observations imply that the reflection at the surface is

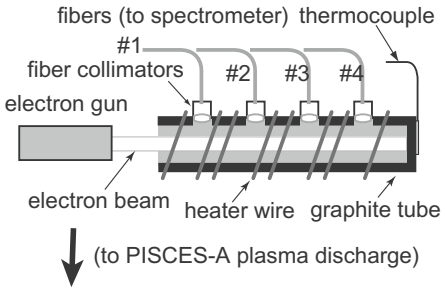

Fig. 1. Close-up of graphite tube mounted in side port.

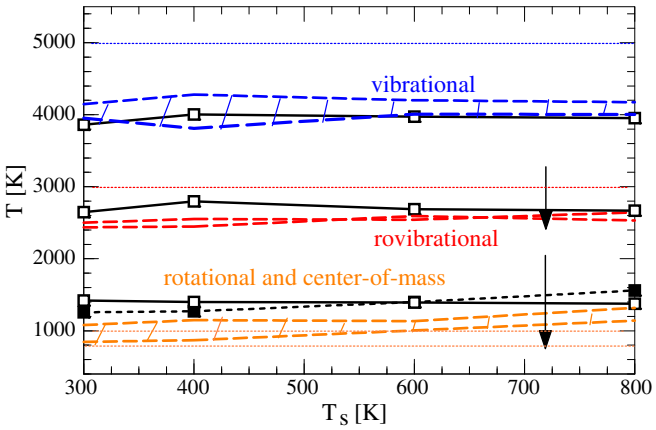

Fig. 2. Post-collisional temperatures of reflected H_2 as a function of the surface temperature. The curves for hydrogenated surfaces are shown by shaded areas between dashed lines, while the bare surface results are displayed by the thick solid lines with open symbols. The center-of-mass translational temperature is given by the short dashed line with solid squares. The thin doted lines represent temperatures of the impacting H_2 molecules. The arrows indicate the direction in which the results change with increasing level of hydrogenation.

accompanied by the conversion of part of the vibrational (and surface) energy into translational and rotational energy. The molecule is also cooled down rovibrationally in the collision, and this effect increases with hydrogenation, similarly to the rotational temperature.

Fig. 3 shows the change in energy of the various modes of H_2 in the collision with the surface, consistent with the discussion in Fig. 2. The positive sign of the energy change for the rotational and c.m. energy is consistent with a negative accommodation coefficient for these modes of motion in the simulated system, which is not confirmed by our experiment, as illustrated in Fig. 5. Quite possible is that the coupling (mixing) of vibrational and rotational modes of motion, obtained here classically, is quantum-mechanically suppressed due to a large energy difference of the vibrational energy levels and the low level of vibrational excitation. Therefore, our simulation results should be accepted with reserve when considering separate rotational and vibrational modes, and considered

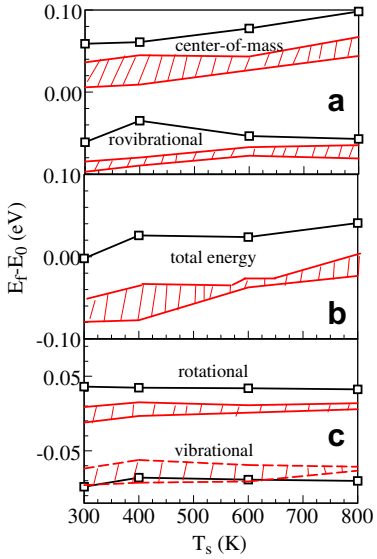

Fig. 3. Energy transfer of the different modes of motion from H_2 molecules in a collision with bare (solid thick line with symbols) and hydrogenated surfaces of various temperatures.

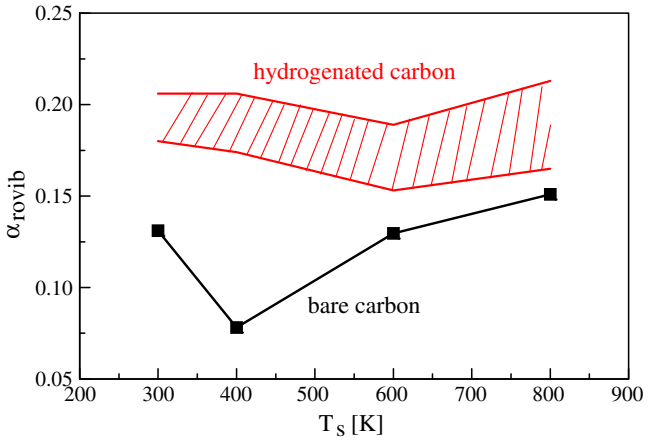

Fig. 4. The rovibrational accommodation coefficient for bare and hydrogenated surfaces, at various surface temperatures. The description of the lines is the same as in Fig 2.

mainly for the conclusions on their sum, the rovibrational energy, which is here, unlike separate rotational and vibrational energies, a conserved quantity. The accommodation coefficient $\alpha_{rovib} = (T_f - T_i)/(T_s - T_i)$, for rovibrational motion upon collision of H_2 with the surface is shown in Fig. 4. $T_{f,i}$ are final and initial rovibrational temperatures of the molecule, while T_s is the surface temperature. It shows a trend of increase with the level of hydrogenation, consistent with higher energy transfers in collisions with lighter particles. Due to the large difference between the vibrational and rotational temperatures, α_{rovib} is dominated by the largest temperature (vibrational). Interestingly, calculated accommodation coefficients are within the uncertainty margins of the experimental results below.

To interpret the measurements, Monte Carlo modeling of H_2 neutral trajectories is used [7]. The free parameters in the modeling are the temperatures $T_{vib,0}$ and $T_{rot,0}$ at the tube entrance and the accommodation coefficients α_{rot} and α_{vib}. Wall collisions are assumed to be diffuse. The kinetic temperature is assumed to be always equal to the rotational temperature, $T_{kin} = T_{rot}$, as is seen in the experiments. Because T_{vib} is found to be much larger (factor of 5-10) than T_{rot}, direct mixing between T_{rot} and T_{vib} in wall collisions is assumed to be small and is neglected. Neutral–neutral collisions and rovibrational energy transfer between vibrational energy and kinetic/rotational energy in these collisions is included in the Monte-Carlo modeling. Neutral density is obtained from the

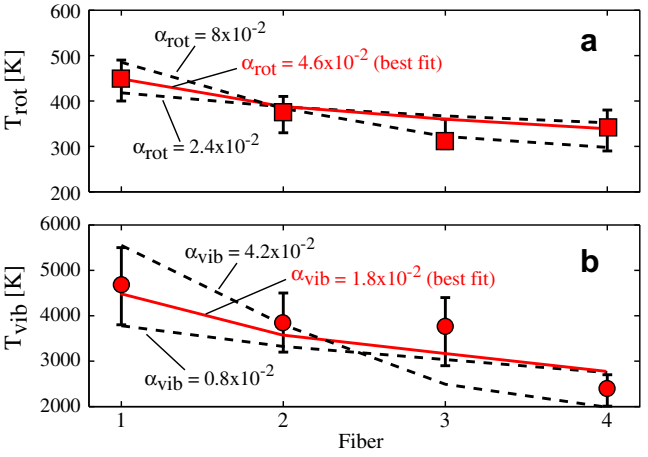

Fig. 5. Monte-Carlo fits (lines) of experimental data (symbols) for (a) T_{rot} vs axial position and (b) T_{vib} vs axial position (see text for a description of the lines).

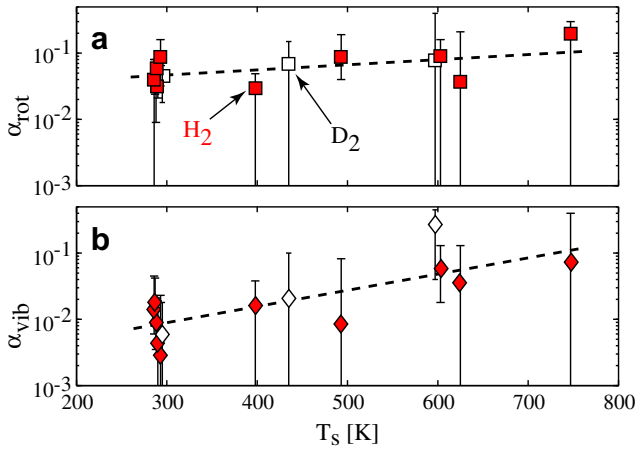

Fig. 6. Measured (a) rotational accommodation coefficients and (b) vibrational accommodation coefficients as a function of surface temperature T_s. Dashed lines are fits through the data. Shaded symbols are for H_2 and white symbols are for D_2.

brightness of the H_2 lines; this is found to depend dominantly on the temperature of the graphite tube. The standard definition of the accommodation coefficient is used [8], i.e. after a wall collision the new rotational temperature is $T'_{rot} = T_{rot} - \alpha_{rot}(T_{rot} - T_s)$, where T_s is the surface temperature. An analogous definition is used for α_{vib} .

Fig. 5 gives an example of Monte-Carlo fits to the measured T_{rot} and T_{vib}. The experiment shown here was for room-temperature graphite. The free parameters $T_{rot,0}$, $T_{vib,0}$, α_{rot}, and α_{vib} were varied to obtain a best fit shown by the solid lines. The error in the accommodation coefficients was estimated by finding the highest and lowest values of α_{rot}, and α_{vib} which would still fit the data within the error bars; these extreme fits are shown by the dashed curves in Fig. 5. Error bars on T_{rot} and T_{vib} data are estimated from the quality of the single-temperature Boltzmann fits to the line populations.

Fig. 6 shows the values of the accommodation coefficients α_{rot} and α_{vib} obtained from various experimental runs (e.g. each point in Fig. 6 corresponds to a fit such as shown in Fig. 5). Overall, the rotational accommodation α_{rot} can be seen to be somewhat $2-10\times$ larger than the vibrational accommodation α_{vib}. Within the scatter of the data, D_2 accommodation (white symbols) is similar to H_2 accommodation (shaded symbols). A slight increase in accommodation with increasing surface temperature is suggested by the data.

Acknowledgments

We acknowledge support by the OFES (P.S.K.) and the OBES (C.O.R.) of the US DOE Contract No. DE-AC05-00OR22725 with UT-Battelle, LLC, and partial support through SciDAC and INCITE projects. SJS acknowledges support by the DOE (DEFG0201ER45889), the NSF (CHE0239448) and a MURI managed by the ARO. E.M.H., R.P.D., D.N. and A.Yu.P. acknowledges support of US DOE Contract Nos. DE-AC02-76CH0307 and DE-AC05-00OR22725. We thank T. Holoman, D. Labrie, P. Roney, J. Timberlake and the NSTX team for technical assistance.

References

[1] P.S. Krstic, C.O. Reinhold, S.J. Stuart, New J. Phys. 9 (2007) 219.
[2] P.S. Krstic, C.O. Reinhold, S.J. Stuart, Europhys. Lett. 77 (2007) 33002.
[3] F.W. Meyer, P.S. Krstic, L.I. Vergara, H.F. Krause, C.O. Reinhold, S.J. Stuart, Phys. Scr. T128 (2007) 50.
[4] D.M. Goebel, G. Campbell, R.W. Conn, J. Nucl. Mater. 121 (1984) 27.
[5] B.P. Lavrov, A.S. Melnikov, M. Kaening, J. Roepcke, Phys. Rev. E 59 (1999) 3526.
[6] Z. Qing, D.K. Otorbaev, G.J.H. Brussaard, et al., J. Appl. Phys. 80 (1996) 1312.
[7] E.M. Hollmann, A. Yu, Z. Pigarov, Z. Yan, J. Nucl. Mater. 363 (2007) 359.
[8] F.O. Goodman, H.Y. Wachman, Dynamics of Gas-surface Scattering, Academic, New York, 1976.